Multichannel far-infrared phase imaging for fusion plasmas

P. E. Young, D. P. Neikirk,[a] P. P. Tong,[b] D. B. Rutledge,[b] and N. C. Luhmann, Jr.

School of Engineering and Applied Science, University of California, Los Angeles, California 90024

(Received 9 July 1984; accepted for publication 1 August 1984)

A 20-channel far-infrared imaging interferometer system has been used to obtain single-shot density profiles in the UCLA Microtor tokamak. This system differs from conventional multichannel interferometers in that the phase distribution produced by the plasma is imaged onto a single, monolithic, integrated microbolometer linear detector array and provides significantly more channels than previous far-infrared interferometers. The system has been demonstrated to provide diffraction-limited phase images of dielectric targets.

INTRODUCTION

There is currently considerable need for accurate measurements of the electron density profile in magnetically confined plasmas with both high spatial and temporal resolution as the profile is directly related to both equilibrium and stability. The most commonly employed technique is optical interferometry whereby the electron density is determined indirectly from a measurement of the plasma dielectric constant.[1] In the simplest case of a cold, unmagnetized plasma the dielectric constant is given by

$$\epsilon(r) = 1 - \omega_{pe}^2(r)/\omega^2 = 1 - n_e(r)/n_c, \qquad (1)$$

where $n_e(r)$ is the electron density, ω is the probing frequency, $\omega_{pe}^2 = 4\pi n_e(r)e^2/m_e$, and n_c is the so-called critical density where $\omega = \omega_{pe}$. Both Mach–Zehnder- and Michelson-type interferometers have been used to measure the phase shift (relative to a vacuum reference path) of an electromagnetic probe beam passing through the plasma and from this the electron density can be inferred.

The choice of operating wavelength for fusion plasma interferometers is governed by a number of factors.[1,2] First, one wishes to operate at as short a wavelength as possible to ameliorate the effects of refraction (angular deflection of the probe beam due to density inhomogeneities) and diffraction (which detrmines the minimum spot size and, hence, the spatial resolution, as well as measurement errors due to phase averaging over the beam cross section). However, there are additional reasons for operating at as long a wavelength as possible. These include the reduction of errors due to machine induced vibrations which can change the path length on the time scale of the density measurement as well as fringe counting errors when the total phase shift is small. The above criteria result in a choice of optimum probe wavelength in the far infrared (FIR) with $\lambda_0 \simeq 100$–$200\ \mu$m for tokamak and mirror fusion devices.

As will be demonstrated in detail in Sec. I, the requirement for spatially resolved density profiles dictates the need for measurements along a large number of chords through the plasma or, in other words, multichannel interferometers. Conventional interferometers employ discrete beams to probe the plasma; because of this such multichannel systems possess a limited number of channels. Basically, the number of channels is limited to $\simeq$5–10 by the expense and complexity of the optical system, as well as by the size, fragility, and cost of detectors (which are typically quasioptical GaAs Schottky diode mixers[3–6]). Examples of far-infrared multichannel interferometer systems using discrete beams include nine channels planned for the Lawrence Livermore National Laboratory MFTF-B tandem mirror,[7] ten planned for the Princeton TFTR tokamak,[8] eight operating on the French TFR tokamak,[9] eight planned on the JET tokamak[10,11], five installed on the Oak Ridge ISX-B tokamak,[12] six planned for the University of Texas TEXT tokamak,[13] and nine operating on the German TEXTOR tokamak.[4]

An approach which surmounts the above mentioned difficulties is phase imaging of the plasma onto a single, integrated monolithic detector array using the system shown schematically in Fig. 1. In addition to reducing the cost and complexity of the optical system, the detector arrays provide increased reliability over discrete whisker–contacted Schottky diode mixers. The advantages associated with this approach have been demonstrated by Hugenholtz and Meddens[15] in a pilot experiment in which they imaged the density profile of a high density resistive arc plasma using a CO_2 laser beam and a 16-element PbSnTe detector array. However, as discussed above, the optimum wavelength choice is in the far infrared. Nevertheless, prior to the recent development of sensitive, monolithic integrated microbolometer detector arrays[16–18] which provide diffraction-limited performance in the FIR, it was not possible to construct such an imaging system. In the present work we described the first phase imaging measurements using a 36-element linear detector array with 20 of the elements actually employed for the tokamak studies. Because of the small size (minor diameter $\simeq$20 cm) and relatively low plasma current ($\simeq$60 kA) in the UCLA Microtor tokamak an operating wavelength of

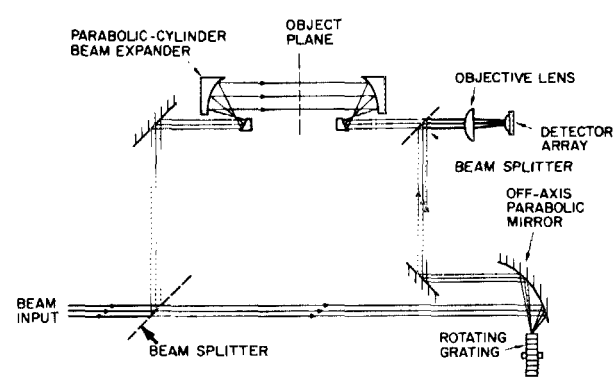

FIG. 1. Schematic of the phase imaging system.

Downloaded 04 Apr 2006 to 131.215.240.9. Redistribution subject to AIP license or copyright, see http://rsi.aip.org/rsi/copyright.jsp

800 μm was chosen for the pilot experiment described here. This wavelength choice is not limited by the detectors as they are extremely broadband (dc to the infrared) and arrays have been shown to provide high resolution imaging at wavelengths as short as 119 μm. To gain confidence in the plasma imaging measurements, the system resolution has also been verified using various dielectric test objects.

The organization of the paper is as follows: Section I contains a discussion of the accuracy of Abel inversion procedures when only a finite number of chordal measurements are available. In addition, details of diffraction-limited imaging are presented together with information concerning the appropriate sampling criteria. The experimental arrangement is described in Sec. II. Results of the system calibration using dielectric test objects are contained in Sec. III. Finally, the use of the system to obtain single-shot time resolved tokamak density profiles is presented in Sec. IV.

I. THEORETICAL CONSIDERATIONS

Several considerations are important in multichannel phase imaging systems such as the plasma interferometer described in the present work. First, the spacing between detectors should be small enough that resolution is limited by diffraction in the optics. There should also be enough channels to reconstruct densities from line-averaged measurements. This calculation is done by an Abel inversion procedure, and the accuracy depends critically on the asumptions made, the number of channels, and the accuracy of the data.

For our imaging system, the maximum detector spacing for diffraction-limited resolution is simply stated. Because the phase is measured, the appropriate spacings are those for electric field detection. The maximum spacing s is then given by[19]

$$s = f^{\#}\lambda_d/n, \tag{2}$$

where $f^{\#}$ is the effective f number of the polyethylene objective lens (see Fig. 1), λ_d is the wavelength in the quartz substrate, and n is the refractive index of the quartz substrate lens. Note that the effective f number is found by projecting the smallest aperture in the entire optical system onto the actual objective lens. In our measurements, $s = 300$ μm, $f^{\#} = 1.5$, $\lambda_d = 400$ μm, and $n = 2$, and this sampling criterion is satisfied.

Since we are interested in obtaining plasma density profiles with high resolution, it is necessary to understand the resolution limits of the imaging system. As will be discussed in Sec. III, these were determined experimentally by imaging dielectric test objects with sharp edges which poses a much more severe test than anything contemplated in the plasma measurement. To aid in understanding these results it is appropriate to consider here the predicted image for such a test object. First note that the image formed by an optical system is a band limited reproduction of the object. Applying the Whittaker–Shannon sampling theorem[20] to this system yields the result that a band limited function can be recovered provided that the function is sampled at regular intervals separated by a distasnce $1/2f_c$, where f_c is the spatial cutoff frequency. The reconstruction algorithm given by this theorem is

$$g(x) = \sum_{n=-\infty}^{\infty} g(n/2f_c)\,\mathrm{sinc}[2f_c(x - n/2f_c)], \tag{3}$$

where $g(n/2f_c)$ are sampled data values.

We also consider how the number of channels affects the accuracy of the Abel inversion procedure used to obtain the plasma density profile from chord-averaged measurements. In practice, one measures the phase shift $\phi(y)$ which is related to the electron density by an integral equation

$$\phi(y) = \frac{\pi}{\lambda n_c}\int_{-L}^{L} n_e(1)d\,1. \tag{4}$$

If one assumes a particular functional form for the density profile then the required number of chordal measurements can be small. For instance, if a parabolic profile is assumed, then one requires only three points. In general, the plasma will not have this shape and will not necessarily be centered in the vacuum vessel. In the coming generation of shaped tokamak plasmas, the density profiles will be deliberately produced with more complicated shapes. More information can be gained if we can reduce the number of assumptions about the density profile. In order to do this a larger number of samples must be obtained.

To illustrate the dependence of the Abel inversion on the number of data points we use the following procedure: Functions which could be analytically inverted were used to represent possible density profiles. If we make the assumption that the profile is axisymmetric (later we will relax this assumption when treating actual data), then the density distribution $n_e(r)$ is related to the measured phase shifts by

$$n_e(r) = \frac{\lambda n_c}{\pi}\int_r^R \frac{d\phi(y)}{dy}\,\frac{dy}{(y^2 - r^2)^{1/2}}. \tag{5}$$

A computer program was used to trace rays through the plasma distribution (the ray tracing routine is based on Ref. 21) and simultaneously calculate the total phase shift using Eq. (1). The resulting phase distribution was Abel inverted using the method of Barr.[22] This method, which has been in use for some time, was chosen because it contains a consistent method for applying a least-squares smoothing of experimental data, and it contains only simple assumptions: (1) the density profile is axisymmetric, and (2) the slope of the profile on axis is zero. Figure 2 shows the inverted data (*) for 20, 10, and 5 data points on one side of the plasma compared with the analytically inverted function (solid line); the function in this case is the Gaussian

$$n_e(r) = \exp(-4r^2/a^2). \tag{6}$$

The increasing error (with decreasing number of data points) is related to the inaccuracies produced in numerically evaluating integrals with a limited number of steps. The integral which is evaluated (and which is included in Barr's method) is that of Eq. (2). Figure 3 shows the same information as Fig. 2 except that the function chosen is

$$n_e(r) = 1 + 10r^2 - 23r^4 + 12r^6, \tag{7}$$

which represents a hollow density profile. In this case, five points are inadequate to recover the density profile. This is because the density profile is represented by a polynomial

Downloaded 04 Apr 2006 to 131.215.240.9. Redistribution subject to AIP license or copyright, see http://rsi.aip.org/rsi/copyright.jsp

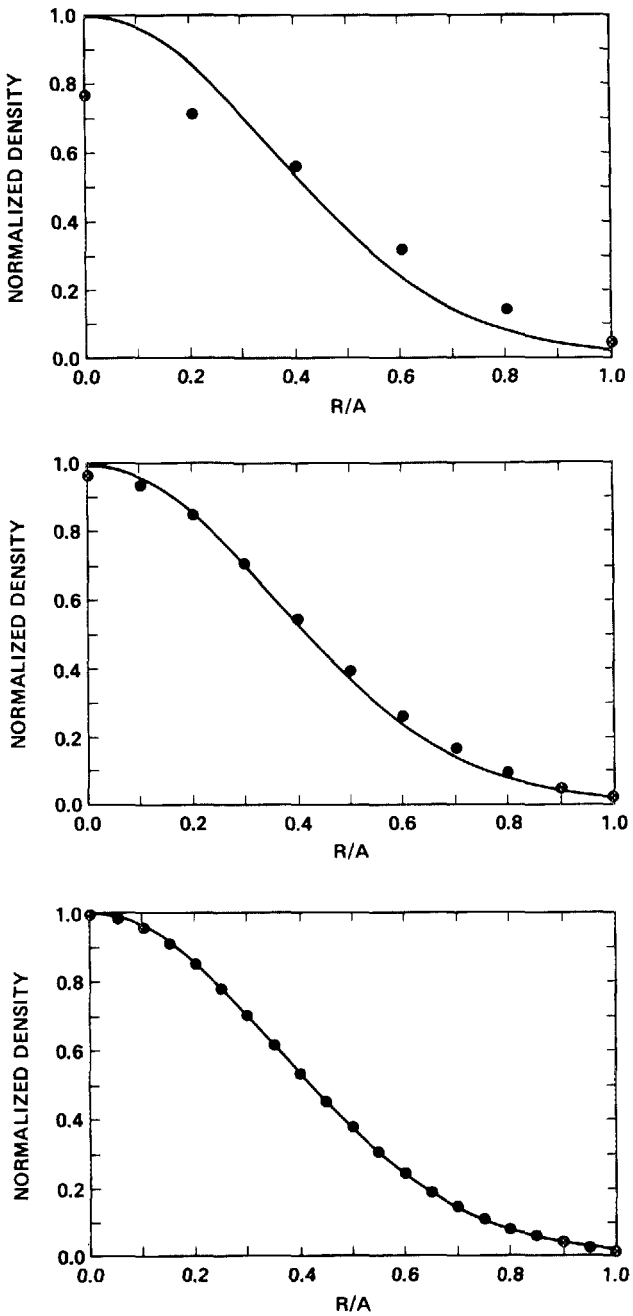

FIG. 2. Numerically inverted data (*) compared to analytically inverted data (solid line) for the function $n_e(r) = \exp(-4r^2/a^2)$ using (a) 20, (b) 10, and (c) 5 points.

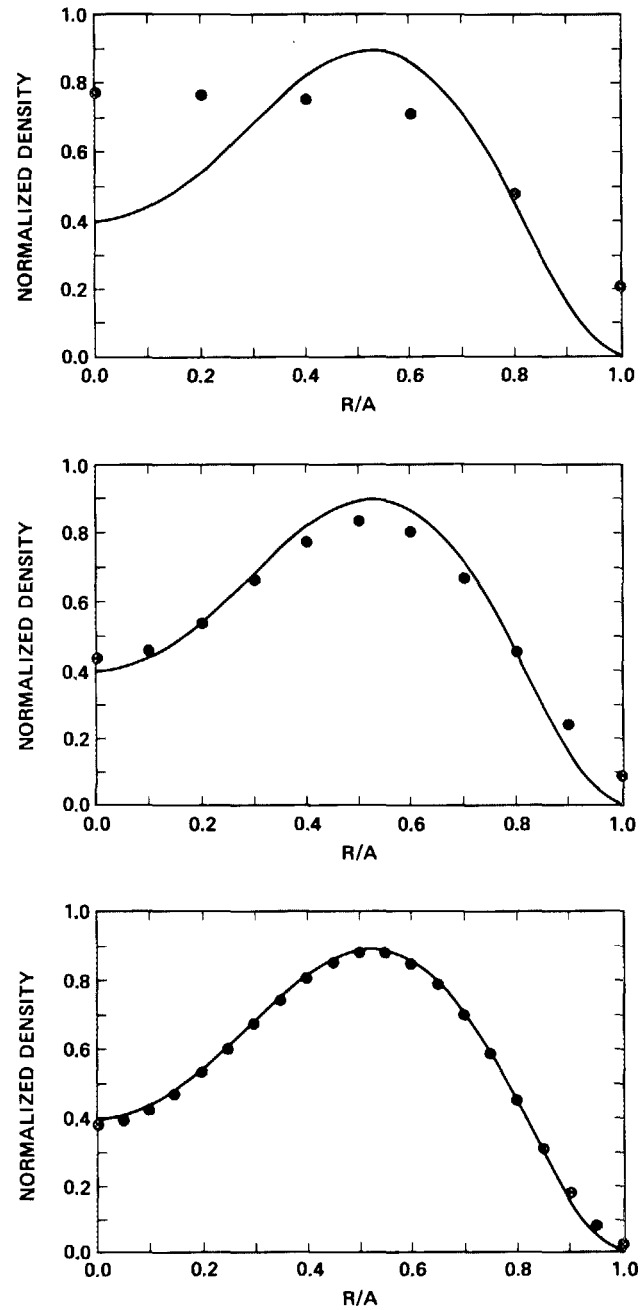

FIG. 3. Numerically inverted data (*) compared to analytically inverted data (solid line) for the function $n_e(r) = 1 + 10r^2 - 23r^4 + 12r^6$ using (a) 20, (b) 10, and (c) 5 points.

whose order is higher than the number of sampled data points.

II. DESCRIPTION OF THE APPARATUS

The interferometer configuration used to measure the plasma line density profile in the UCLA Microtor tokamak is shown in Fig. 4. The optics are configured as a heterodyned Mach–Zehnder interferometer. The reference arm is Doppler shifted 85 kHz in frequency by a rotating grating.[23] The source is a Thomson-CSF carcinotron (O-type backward wave oscillator)[24] operating at 800 μm. The probe beam is expanded in one dimension by a pair of cylindrical lenses resulting in efficient transmission through the tokamak vacuum port and illumination of the entire plasma cross section. The diameter of the plasma vessel is 22.4 cm and the tokamak ports are roughly rectangular (21 cm long by 3 cm wide) allowing an unobstructed view across the plasma. Anther pair of cylindrical lenses located outside the plasma vessel (and following the probe beam exit window) reshapes the probe beam to match the reference beam profile. A combination of a concave cylindrical lens and a convex aspheric objective lens forms a line image at the detector array.

The total efficiency of the optical system is approximately 22% which compares favorably with a maximum efficiency of 50% for a Mach–Zehnder interferometer. Table I lists the components of the interferometer which contribute significant power loss. The most significant loss is

Downloaded 04 Apr 2006 to 131.215.240.9. Redistribution subject to AIP license or copyright, see http://rsi.aip.org/rsi/copyright.jsp

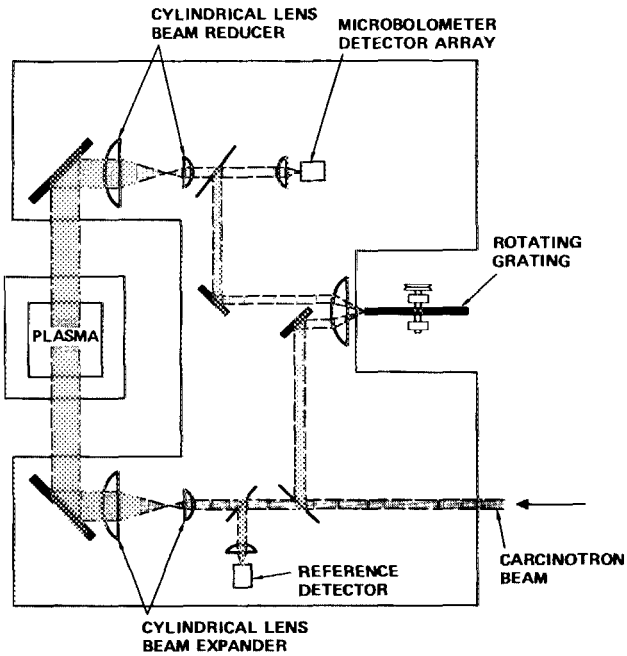

FIG. 4. Tokamak imaging system.

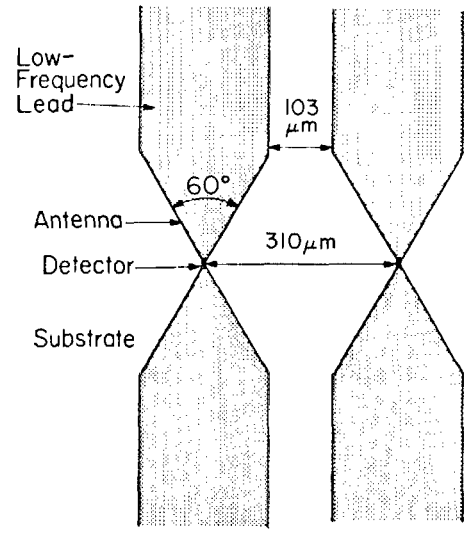

FIG. 5. Imaging array antenna design for a wavelength of 800 μm.

caused by absorption in the lens material. All lenses are constructed of high-density polyethylene; we have estimated the absorption loss to be 0.3 dB/cm (by comparing the power levels measured by a Scientech model 362 calorimeter with the FIR beam blocked and unblocked by a polyethylene slab of known thickness) which compares favorably to values given in the literature.[24] The loss in the cylindrical lenses includes both the absorption loss as well as a 4% reflection loss at each surface. The loss at the rotating grating is again due to absorption loss in the focusing lens; replacing the grating with a plane mirror does not significantly change the transmitted power. The tokamak windows are 1.2-cm-thick polyethylene. Power loss due to the finite size of the tokamak ports is avoided by using cylindrical lenses to form a beam waist at the center of the plasma. Typical output power from the carcinotron is 10 mW; for the given system efficiency and 20 detectors, approximately 100 μW reaches each detector on an average.

The imaging array is a monolithic integrated circuit specially developed for plasma diagnostics.[16,17] Figure 5 shows the design consisting of a line of bow-tie antennas with bismuth microbolometer detectors on a fused-quartz substrate. The spacing between the antennas is 310 μm, which corresponds to three-quarters of the wavelength in quartz. The bolometers rest on a 2-μm-thick polyimide film that reduces the thermal conductance to the substrate. At the modulation frequency of 85 kHz, the bolometers are limited by Johnson noise and have an electrical noise equivalent power (NEP) of 6×10^{-11} W/Hz$^{1/2}$ (Ref. 27). The entire array consists of 36 antennas and bolometers and mounts in a standard integrated-circuit package. The far-infrared beam is coupled through the substrate by a fused-quartz lens (Fig. 6). This substrate lens eliminates surface-wave losses and takes advantage of the fact that antennas on a substrate are more sensitive to radiation that comes through the substrate than to radiation impinging directly from the air.

Since the detectors are separated by 310 μm on the substrate, to obtain one sample per centimeter over the 20-cm plasma diameter we require a magnification of 33. For this optical system, the substrate lens produces a magnification of four and the two cylindrical lenses (focal lengths of 12.7 and 38.1 cm) yield a magnification of three. The remaining magnification is provided by the aspheric objective lens. The array is placed at the calculated image plane for an object plane located at the plasma center which is 1.17 m in front of the first cylindrical lens. It has been noted that imaging the plasma in this manner will compensate for errors in the phase shift due to refraction.[28] The two lenses before the plasma affect the image only in that they will determine how the amplitude of the probe beam is distributed over the object plane.

TABLE I. Optical components contributing to power losses of over 5%. Total power loss = 7.8 mW, total power input = 10.0 mW, total efficiency = 22%.

Optical Elements	Power loss (mW)
(1) Four cylindrical lenses	4.2
(2) Rotating grating	0.4
(3) Tokamak ports	0.5
(4) Last beam splitter	2.7

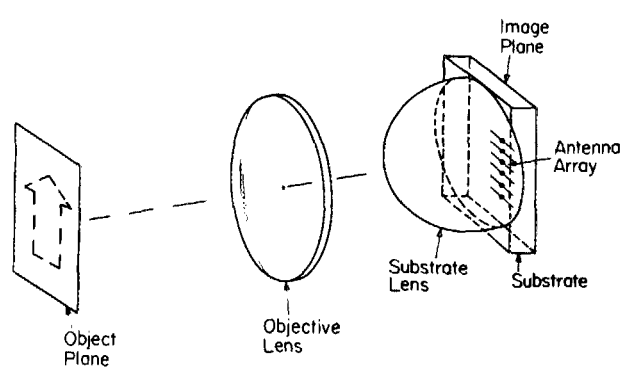

FIG. 6. Optical arrangement for imaging onto the detector array. Note that the array substrate is between the array and the objective lens.

Downloaded 04 Apr 2006 to 131.215.240.9. Redistribution subject to AIP license or copyright, see http://rsi.aip.org/rsi/copyright.jsp

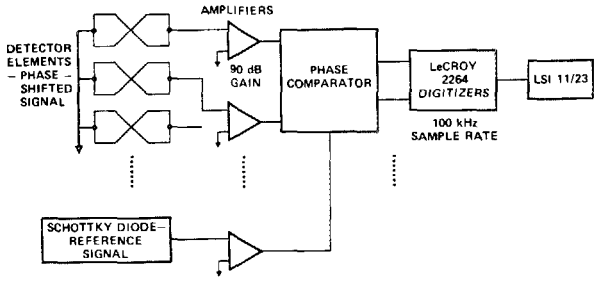

FIG. 7. Signal processing arrangement for the interferometer measurement using the microbolometer detector array.

The output of the detector array is processed by the electronics shown schematically in Fig. 7. The signal from each detector is amplified by separate amplifiers with 90-dB gain and 2.5-dB noise figure and an operating bandwidth between 20 kHz and 1.7 MHz. The interferometer signal is filtered with a bandwidth of 30 kHz about an 85-kHz center frequency. A digital phase comparator of conventional design[29] compares the phase of the signal from each detector with the phase of the reference signal sensed by a quasioptical GaAs Schottky diode mixer of either the biconical[3,4] or corner-cube design.[5,6] The output of the phase comparator is a voltage which is proportional to the phase shift. This signal is sent to a LeCroy model 2264 waveform digitizer. The digitizers are typically run in the eight-channel mode with 8 kbytes of memory per channel at a 100-kHz sample rate. An LSI 11/23 computer is used to automatically acquire the data and for data processing after each shot.

III. HOLOGRAPHIC IMAGING OF DIELECTRIC PHASE OBJECTS

We would like to demonstrate the ability of the imaging system to reconstruct known phase distributions. In this section we will show the results of imaging two different types of dielectric phase objects: (1) a cylindrical lens with a spatial frequency much less than the optical cutoff frequency, and (2) a dielectric bar which produces spatial frequencies above the optical cutoff frequency.

Figure 8 shows the phase image of a cylindrical lens compared with the theoretically predicted phase distribution. The lens is planoconvex, is made of polyethylene, and has a front surface curvature of 24 cm. This phase distribution is used to represent an object with spatial frequencies much less than the sampling frequency; typical plasma profiles will have a similar phase distribution. Since the image is not diffraction limited, we can calculate the expected phase distribution by using geometric optics to calculate the phase change of rays passing through the lens.

Imaging an object with sharp edges tests the resolution limit of the system. In Fig. 9(a) we show the measured phase image of a polyethylene bar of width 2.5 cm and thickness 0.81 mm—this produces a phase shift of 1.02π. The drawn line has been calculated from the measured data using the interpolation formula, Eq. (3). Using the optical cutoff frequency f_c calculated in Sec. I, we can calculate the phase distribution by first Fourier-transforming the spatial pulse function into the frequency domain, filtering out all frequency components above f_c, and then transforming back to the spatial domain. This results in a phase distribution

$$\phi(x) = (2/\pi)^{1/2}\phi_0\{\mathrm{Si}[2\pi f_c(x+a)] - \mathrm{Si}[2\pi f_c(x-a)]\}, \tag{8}$$

where Si is the sine integral,[30] ϕ_0 is the pulse height, and $2a$ is the width of the bar. This function is shown in Fig. 9(b) and can be compared with the interpolated phase data; there is good agreement between the two.

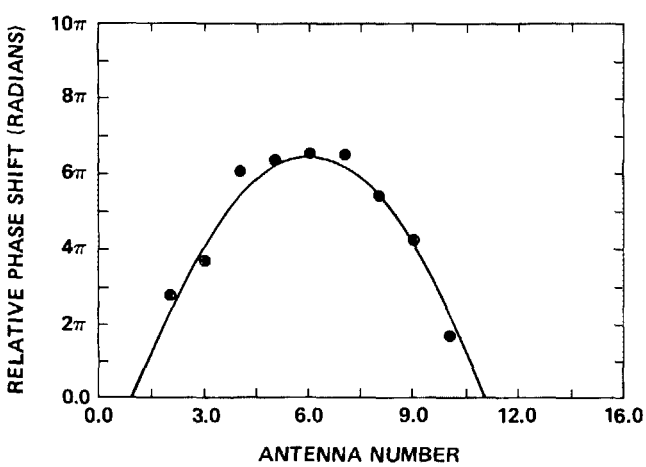

FIG. 8. Image of a cylindrical lens compared to the theoretically predicted phase distribution.

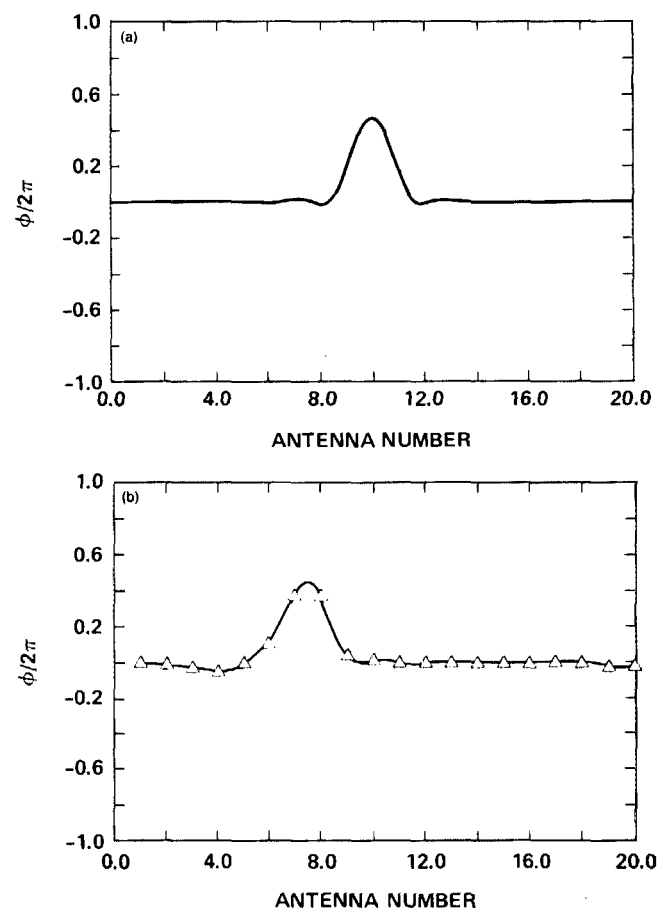

FIG. 9. Comparison of (a) theoretically predicted phase image of a dielectric bar, and (b) actual recorded image of a bar located on the optic axis.

Downloaded 04 Apr 2006 to 131.215.240.9. Redistribution subject to AIP license or copyright, see http://rsi.aip.org/rsi/copyright.jsp

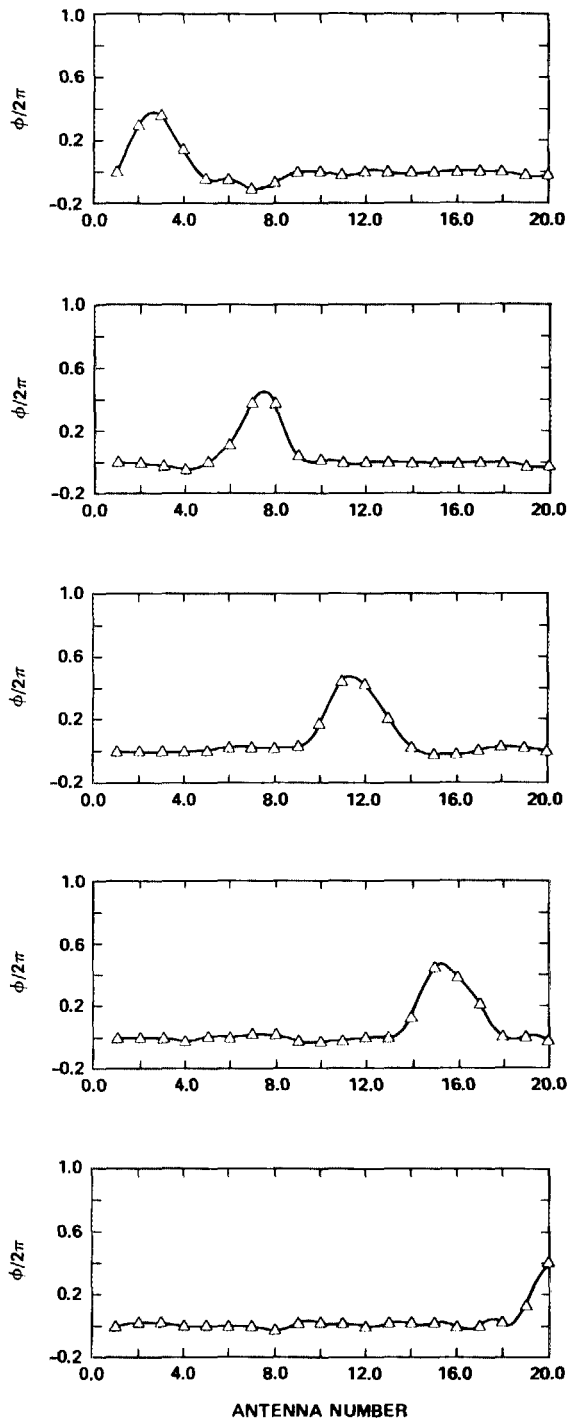

FIG. 10. Image of a Teflon bar (2.5 cm×0.81-mm thick) recorded by the detector array at positions (a) $x = -6$ cm, (b) $x = -2$ cm, (c) $x = 2$ cm, (d) $x = 6$ cm, and (e) $x = 10$ cm.

Using the bar target we can easily test the optical system to correlate object plane spatial position with antenna number and also test the magnification of the system. Figure 10 shows the image of the bar target as it is moved across the object plane. The bar target was moved 4 cm between views; this shifts the position of the image by two detectors confirming the designed magnification of the system. We can also test for serious aberration effects by looking for a change in resolution as a function of object position in the direction transverse to the optic axis. While diffraction limits the image bandwidth, aberrations can produce distortions of the system response within the passband. Note that the bar image shows minimal distortion as it is moved across the object plane and, more importantly, appears at the expected spatial position with the predicted maximum phase value.

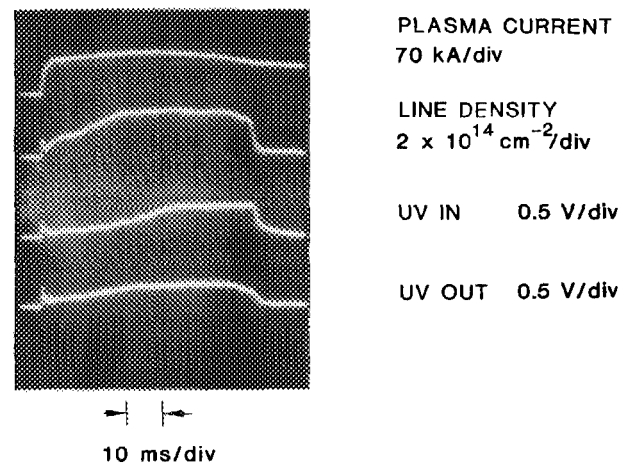

FIG. 11. A typical Microtor discharge. Shown are (a) total plasma current, (b) central line density, and ultraviolet emission monitored by detectors, (c) 6 cm inside the vessel center, and (d) 6 cm outside the vessel center.

IV. TOKAMAK RESULTS

The system described above was used to obtain density profiles in the UCLA Microtor tokamak. This device has a minor radius of 11.2 cm, a major radius of 40 cm, a toroidal magnetic field of 20 kG, total plasma current of 60 KA, and central densities which are typically 5×10^{13} cm^{-3}. The discharges can have durations of up to 100 ms. This tokamak is characterized by the traces shown in Fig. 11 which show the total plasma current, central line density, and ultraviolet emission (monitored by detectors located 6 cm either side of the vessel center) for a typical discharge. The gas feed was intentionally shut off at $t = 80$ ms which causes the pronounced drop in density at that time. The line density profile for the same shot during the first 60 ms is shown in Fig. 12.

For the purpose of this article, we would like to illustrate the importance of having many channels; discussion of physics results is deferred to a later publication. Detailed

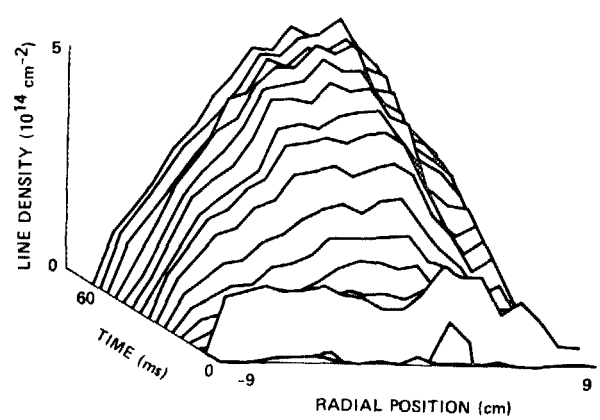

FIG. 12. Measured time development of the line density profile in the UCLA Microtor tokamak.

Downloaded 04 Apr 2006 to 131.215.240.9. Redistribution subject to AIP license or copyright, see http://rsi.aip.org/rsi/copyright.jsp

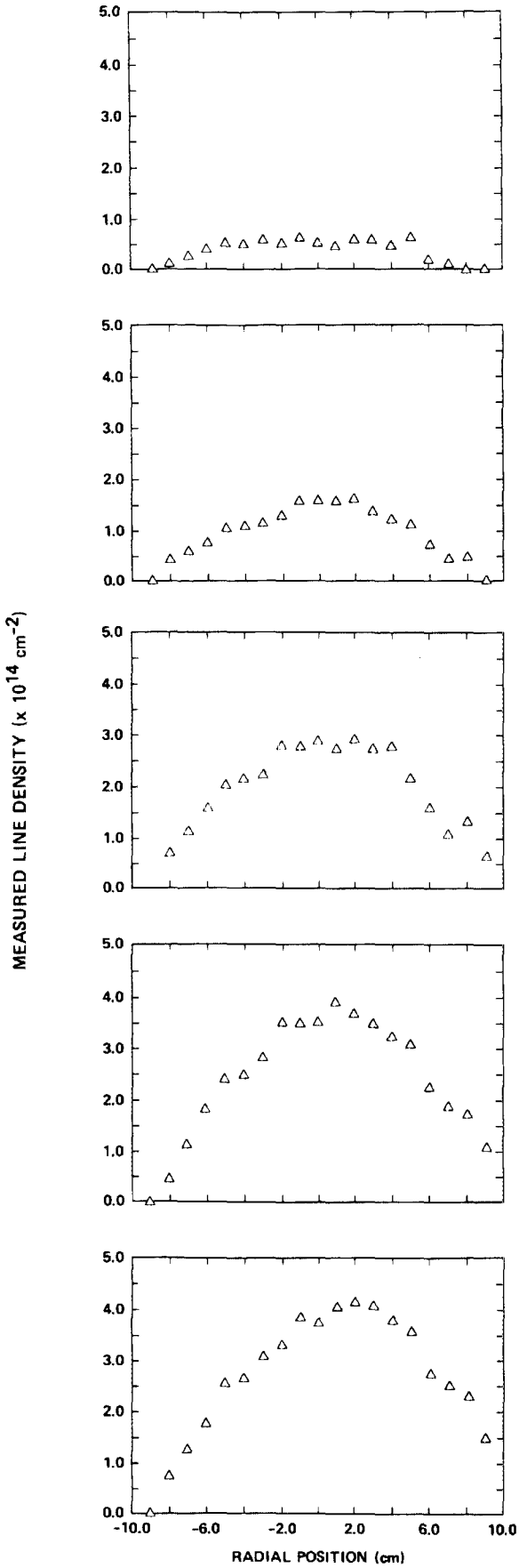

FIG. 13. Selected measured radial line density profiles. The first profile occurs 2 ms after the start of the discharge. Subsequent profiles are separated by 5 ms.

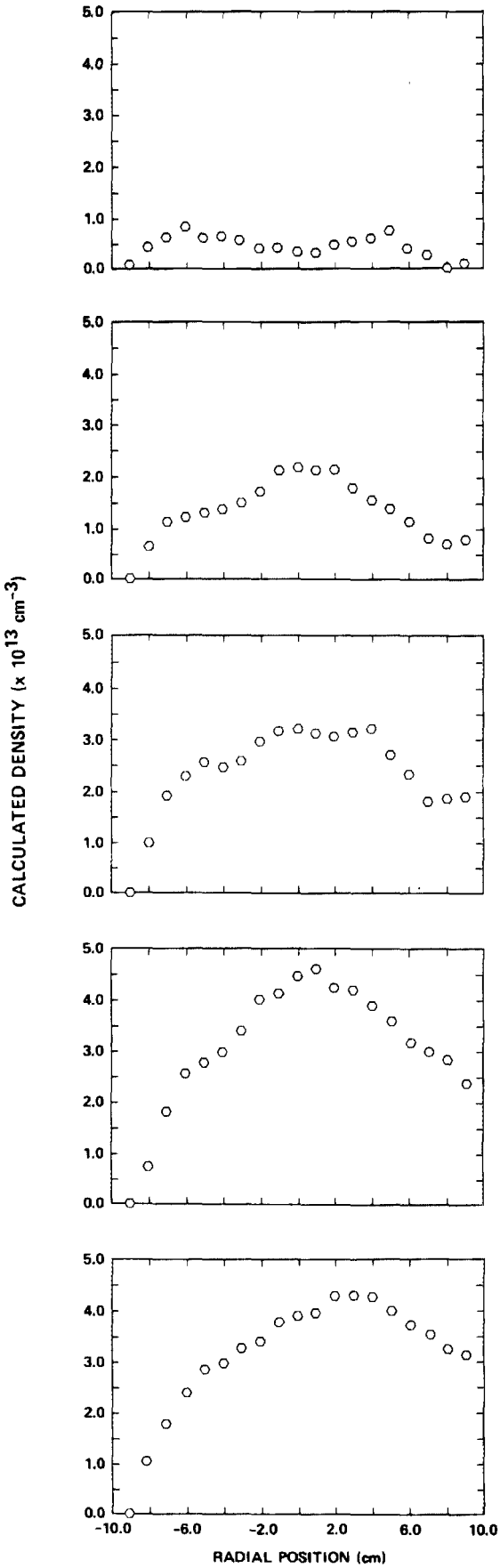

FIG. 14. Radial density profiles calculated from the line density profiles in Fig. 13 using an Abel inversion routine based on Ref. 31.

Downloaded 04 Apr 2006 to 131.215.240.9. Redistribution subject to AIP license or copyright, see http://rsi.aip.org/rsi/copyright.jsp

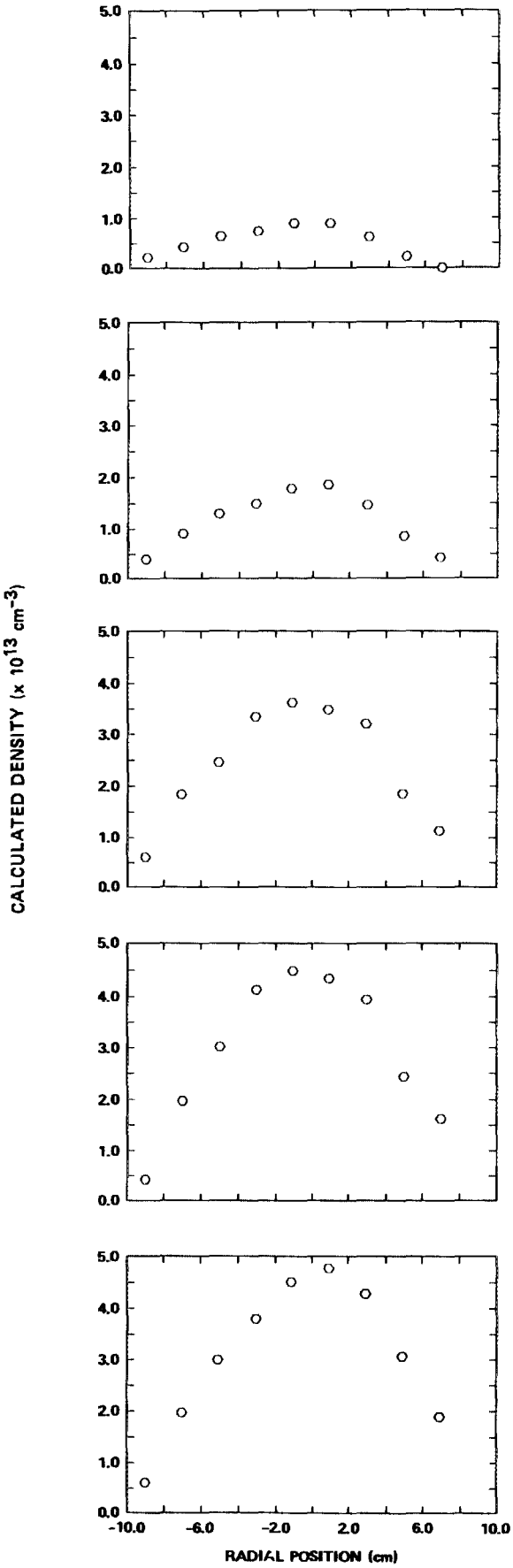

FIG. 15. Radial density profiles calculated from the line density profiles in Fig. 13, but using only alternate data points (for a total of nine data points) to illustrate the advantages of an increased sampling rate.

analysis of the profile shown in Fig. 12 illustrates the advantage of having many channels. Figure 13 shows the line density profiles at times separated by 5 ms; the first profile occurs 2 ms into the discharge. Figure 14 shows the Abel inversion of the profiles shown in Fig. 13. The inversion routine is based on the analysis developed by Yatsutomo *et al.*[31] which allows for asymmetric profiles by assuming the density profile is given by

$$n_e(x,v) = g(y)n_0(r), \tag{9}$$

where $g(y)$ is a weighting function in the direction transverse to the probe beam and $n_0(r)$ is a symmetric function. The symmetric part is obtained from the symmetric part of the line density profile using Barr's inversion method. Note that near the beginning of the shot the density profile is distinctly hollow. This profile rapidly evolves ($\sim$3 ms) into a roughly parabolic shape whose center moves outward as the plasma evolves until it is located 2 cm outside of the vessel center 40 ms into the shot. These results can be compared with the inversions using only nine data points which are shown in Fig. 15. In most cases there is a significant difference, particularly in the earliest profile. Note also the error in the location of the peak density at later times.

We have successfully implemented a 20-channel FIR imaging interferometer using an integrated monolithic detector array to obtain tokamak density profiles. The spatial resolution of the system has been demonstrated as well as the advantage of having a large number of channels. This system can be readily adapted to larger tokamaks by changing the magnification of the imaging optics.

ACKNOWLEDGMENTS

The authors wish to thank Dr. R. J. Taylor for providing machine time and technical support on the UCLA Microtor tokamak. Phillip Hoffman of the UCLA Department of Electrical Engineering designed and built the prototype of the low noise amplifier. The work was supported by the U. S. Department of Energy, Office of Fusion Energy Contract No. DE-AM03-T6SF00010, P. A. No. DE-AT03-T6ET53019, Task IIIB.

[a] Present address: Department of Electrical Engineering, University of Texas, Austin, TX 78712.
[b] Division of Engineering and Applied Science, California Institute of Technology, Pasadena, CA 91125.

[1] D. Veron, in *Infrared and Millimeter Waves*, Vol. II, edited by K. J. Button (Academic, New York, 1979).
[2] A. Nagashima, in Proceedings of the USA–Japan Workshop on Submillimeter Diagnostic Techniques, US-J FRC-006, January 1982.
[3] J. J. Gustincic, Proc. Soc. Photo-Opt. Instrum. Eng. **105**, 40 (1977).
[4] J. J. Gustincic, IEEE MIT-S International Microwave Symposium Digest IEEE 77 Ch 1219-5 MTT, 1977.
[5] H. Krautle, E. Sauter, and G. V. Schultz, Infrared Phys. **17**, 937 (1977).
[6] H. Fetterman, P. E. Tannenwald, B. J. Clifton, C. D. Parker, W. D. Fitzgerald, and H. R. Erickson, Appl. Phys. Lett. **33**, 151 (1978).
[7] J. Monjes and A. Throop (private communication).
[8] D. Mansfield (private communication); also see Princeton Plasma Physics Laboratory TFTR Physics Group Report No. 40, 1981.
[9] D. Veron, J. Certain, and J. P. Crenn, J. Opt. Soc. Am. **67**, 964 (1977).

Downloaded 04 Apr 2006 to 131.215.240.9. Redistribution subject to AIP license or copyright, see http://rsi.aip.org/rsi/copyright.jsp

[10]D. Veron, Proceedings International School on Plasma Physics, Varenna, Italy, 1982.
[11]D. Veron, IEA Workshop on Plasma Diagnostics, Princeton, NJ, March 1980.
[12]D. P. Hutchinson, C. H. Ma, P. A. Staats, and K. L. VanderSluis, Nucl. Fusion **21**, 1535 (1981).
[13]T. R. Price and D. P. Hutchinson, Fourth APS Topical Conference on High Temperature Plasma Diagnostics, paper F8, 1982.
[14]H. Soltwisch, Nucl. Fusion **23**, 1681 (1983).
[15]C. A. J. Hugenholtz and B. J. H. Meddens, Rev. Sci. Instrum. **53**, 171 (1982).
[16]D. P. Neikirk, D. B. Rutledge, M. S. Muha, H. Park, and C.-X. Yu, Appl. Phys. Lett. **40**, 203 (1982).
[17]D. P. Neikirk, P. P. Tong, D. B. Rutledge, H. Park, and P. E. Young, Appl. Phys. Lett. **41**, 329 (1982).
[18]D. B. Rutledge, D. P. Neikirk, and D. P. Kasilingam, in *Infrared and Millimeter Waves*, Vol. 10, edited by K. J. Button (Academic, New York, 1983).
[19]D. P. Neikirk, Ph.D. thesis, California Institute of Technology, 1983.
[20]J. W. Goodman, *Introduction to Fourier Optics* (McGraw–Hill, New York, 1968).
[21]J. Schmoys, J. Appl. Phys. **32**, 699 (1961).
[22]W. L. Barr, J. Opt. Soc. Am. **52**, 885 (1962).
[23]D. Veron, Opt. Commun. **10**, 95 (1974).
[24]G. Kantorowicz and P. Palluel, in *Infrared and Millimeter Waves*, Vol. I, edited by K. J. Button (Academic, New York, 1979).
[25]G. W. Chantry, J. W. Fleming, and P. M. Smith, Chem. Phys. Lett. **10**, 473 (1971).
[26]A. G. Zhukov, Radio Eng. Electron. Phys. **11**, 1489 (1966).
[27]D. P. Neikirk, W. W. Lam, and D. B. Rutledge, Int. J. Infrared Millimeter Waves **5**, 245 (1984).
[28]C. M. Vest, Appl. Opt. **14**, 1601 (1975).
[29]S. M. Wolfe, K. J. Button, J. Waldman, and D. R. Cohn, Appl. Opt. **15**, 2645 (1976).
[30]M. Abramowitz and I. A. Stegun, *Handbook of Mathematical Functions* (Dover, New York, 1965), Chap. 5.
[31]Y. Yatsutomo, K. Miyata, S. Himeno, T. Enoto, and Y. Ozawa, IEEE trans. Plasma Sci. **PS-9**, 15 (1982).

Downloaded 04 Apr 2006 to 131.215.240.9. Redistribution subject to AIP license or copyright, see http://rsi.aip.org/rsi/copyright.jsp